THE JOURNAL OF PHYSICAL CHEMISTRY C
A JOURNAL OF THE AMERICAN CHEMICAL SOCIETY

pubs.acs.org/JPCC

Article

Anomalous Deformation Behavior in ULE Glass upon Microindentation: A Vibrational Spectroscopic Investigation in the Induced Structural Changes of a Ti-Silicate Glass

Published as part of The Journal of Physical Chemistry virtual special issue "Hellmut Eckert Festschrift".

Doris Möncke,* Felix Lind, Brian Topper, and Efstratios I. Kamitsos

Cite This: *J. Phys. Chem. C* 2021, 125, 4183–4195

Read Online

ACCESS | Metrics & More | Article Recommendations

ABSTRACT: Ultralow expansion (ULE) glass, a binary TiO_2–SiO_2 glass with 5.67 mol % TiO_2, was exposed to microindentation. Vitreous silica was similarly treated and used as a reference material, including the characterization of mechanical properties by means of ultrasonic echography and nanoindentation. The structural modifications induced by indentation were analyzed by micro-Raman spectroscopy. The observed structural changes are consistent with an anomalous, densification-driven, deformation mechanism similar to those observed for vitreous silica or commercially relevant low alkali borosilicate glasses like Duran. As for these fully polymerized glasses, the Raman spectra of indents in the ULE glass are characterized by an upshift of the 407 cm^{-1} band and an increase in the intensity of the D_1 and D_2 defect bands, all consistent with structural rearrangements from mostly larger five- and six-member rings to a larger population of smaller four- and three-member rings and an overall lowering of the free volume in the glass. However, contrary to silicon, titanium may change its coordination number under the impact of microindentation. Raman spectra of selected reference materials such as TiO_2 and $BaTiO_3$, with known octahedral titanium coordination and known connectivity, as well as fresnoite $Ba_2TiSi_2O_8$ with known fivefold Ti^{4+} coordination, are therefore included in this study in support of assigning the new activity appearing in the Raman spectra after an indentation of the ULE glass sample.

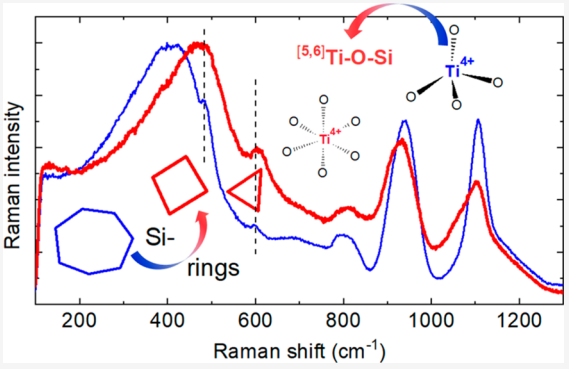

1. INTRODUCTION

For modern glass applications, mechanical properties such as fracture toughness and hardness play a key role and facilitate the design of glasses with mechanically favorable properties. Thus, studies on the correlations of hardness, elasticity, and the glass structure gain increasing attention. Indentation testing is used in the determination of critical loads for crack initiation or fracture toughness.[1−4] While instrumented (nano)indentation testing is now widely used to study deformation mechanisms of glasses ranging from elastic contact to inelastic shear flow, to densification and cracking,[3,5−7] microindentation testing also allows the direct study of structural changes that are a consequence of and response to a mechanical impact.[8−11]

The response of inorganic oxide glasses toward an external force, such as indentation, falls as a rule into one of two categories; the first is the "normal" process by shear-driven deformation, and the second is the "anomalous" process of compaction.[2,3,12−15] The predominance of the latter process, due to an excess in free volume and subsequently enhanced densification, often results in glasses that can withstand enhanced crack initiation loads.

Raman spectroscopy proved to be the method of choice when following structural modifications after indentation, as the spatial resolution of a Raman microscope (0.5−1 μm when using a blue or green laser line) is significantly smaller than, for example, micro-Vicker's indents. Earlier studies focused on pure vitreous silica[16,17] and soda-lime-silicate glasses,[18] later to be augmented by other compositions and various studies on borosilicate glasses.[19] We focused particularly on low-alkali borosilicate glasses, which, like "Pyrex"- or "Duran"-type glasses, are of high technical importance and which, like vitreous SiO_2, exhibit a fully polymerized glass network and fall

Received: November 2, 2020
Revised: January 27, 2021
Published: February 10, 2021

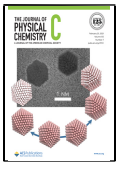

Downloaded via NATL HELLENIC RESEARCH FOUNDATION on March 20, 2023 at 07:38:15 (UTC).
See https://pubs.acs.org/sharingguidelines for options on how to legitimately share published articles.

ACS Publications

© 2021 American Chemical Society

https://dx.doi.org/10.1021/acs.jpcc.0c09865
J. Phys. Chem. C 2021, 125, 4183–4195

in the category of "anomalous" glasses when considering their response toward mechanical testing.[10,11,14,20−22] Another fully polymerized, technically important silicate-rich glass is the Ultra Low Expansion glass (ULE, Corning), a binary titanosilicate glass. With a TiO_2 fraction of 7.4 wt % (5.67 mol %), ULE exhibits an almost zero coefficient of thermal expansion (CTE) from 5 to 35 °C (CTE of 0 (±30) × 10^{-9}/°C), and even between 100 and 300 °C the CTE is an order of magnitude smaller than for vitreous silica.[23] The structure of ULE can be broadly described as vitreous SiO_2 in which less than one of every 18 SiO_4 tetrahedra is replaced by a TiO_4 tetrahedron. This was also confirmed in a recent X-ray diffraction (XRD) study[24] and is in agreement with earlier X-ray absorption spectroscopic studies, which found that, depending on the TiO_2 content, titanium ions may occupy fourfold sites, sixfold sites, or even a fivefold coordination environment.[25,26]

Because of its low CTE, ULE glass is employed in applications requiring a geometrical stability at ambient temperature, such as substrates and mask blanks for lithography or mirror blanks. Additionally, it has been shown that nanogratings can be generated by laser modification of ULE glass, making ULE an interesting candidate for use in optical and imaging operations.[24,27,28] In a laser-modified ULE, the structural modifications were found in the molten glass near the laser-generated cavities and in the surrounding remolten glass.[24,27,28] Contrary to indentation experiments, the energy of the laser beam also causes the partial reduction of Ti^{4+} ions to Ti^{3+}, while some oxygen ions from the glass network are oxidized to molecular oxygen, which is trapped in the formed cavities. For remolten areas in laser-irradiated ULE, our latest and most detailed report on laser-modified ULE[24] shows a densification of the glass network in the shells of cavities similar to that of silica under indentation, in addition to the reduction in density in areas in close proximity of the generated cavities. These laser-induced changes sparked our interest to look also into structural changes of a ULE glass under a purely mechanical impact, where a change in the oxidation state of titanium ions would not be likely. Attempting similar studies as performed earlier on low-alkali borosilicate or vitreous SiO_2 glasses,[10,11,14,21,22,29] we aim at identifying any structural modifications in ULE occurring as a consequence of indentation. While we expect a similar "anomalous" densification-driven behavior as for the other named fully polymerized silica-rich glasses, we may also assume no reduction of titanium ions, contrary to the results of our laser modification studies. However, the ability of titanium ions to lastingly change their coordination from four- to five- to sixfold[25,26,30,31] might offer a new pathway of response in ULE, which is not available for the SiO_2 or a Duran-type network. The importance of a permanent increase in the coordination number of many ions under indentation was discussed previously in detail by Januchta et al.[13] For ULE glass, titanium is expected to differ from boron in Duran. While we suggested an increase in the boron coordination from three to four under indentation, this high-density, higher boron coordination required an increase of oxygen coordination from twofold to threefold.[10] Because of a lack of modifier cations that could stabilize the charge-deficient borate tetrahedra lastingly, the higher coordinations were transient and reverted back to the lower coordination once the pressure of the indentation was released. However, the transient higher-coordinated species did facilitate a shear mechanism and explained the loss of boroxol and borate rings during indentation.[10]

In the present microindentation study of ULE glass, we performed for comparison parallel experiments on commercial v-SiO_2 samples and include selected data from earlier studies on Duran to highlight the similarities and differences between these three fully polymerized silica-rich glasses. Also, for a better understanding of the vibrational response of titanates in higher coordination numbers than four, we present information on Raman bands for higher-coordinated titanate species and include the spectra of some crystalline and amorphous reference titanate materials.

2. EXPERIMENTAL SECTION

All experiments were conducted in the laboratory under air at an ambient temperature of ∼25 °C.

2.1. Samples. The ULE© glass used in this study is commercially available from the manufacturer and has the composition 5.67TiO_2−94.33SiO_2 in mol %.[23,32] For comparison, the well-characterized pure commercial silica glass (Herasil102) is included in the study.[33] Prior to the measurements the glass specimens were polished to an optical finish, resulting in coplanar slides with a thickness d from 1 to 6 mm, which was verified using a micrometer screw with an accuracy of ±2 μm.

Reference materials included commercial titanates such as TiO_2 (anatase) from Acros Organics (99%), dipotassium hexafluoro-titanate K_2TiF_6 from Sigma-Aldrich, and barium titanate $BaTiO_3$ from Sigma-Aldrich (99%). The rutile phase of TiO_2 was prepared by heating anatase on a platinum foil boat in a furnace at 1000 °C for 18 h. The platinum foil boat was removed and allowed to cool in the air. A fresnoite glass was prepared by mixing the appropriate amounts for 8 g of glass of $BaCO_3$, TiO_2, and SiO_2 in a platinum crucible and placing the mixture in an electric furnace at 1500 °C for 30 min. The melt was quenched between two preheated metal plates to yield a transparent glass. Two pieces of an equivalent apparent size and thickness were selected from the same cast. One was set aside, without further annealing. The other glass piece was devitrified by placing it on a flat platinum foil square and placing this in an electric furnace at 1250 °C for 90 min and then removing it to cool in the air.

2.2. Glass Properties. The glass density ρ was measured by Archimedes' method using deionized water as the immersion liquid. Data sheets from Corning[32] and Heraeus[33] are also available for the properties of ULE and v-SiO_2, respectively.

2.3. Mechanical Testing. The mechanical properties were examined by ultrasonic echography, nanoindentation, and microindentation. Not only atmospheric humidity but also the time factor between indentation and observation does affect, for example, the crack resistance and other properties, as shown in previous studies.[7,34,35] For ULE glasses, prior to testing, no significant degradation is expected over time for carefully stored polished glass pieces. Mechanical testing was conducted at ambient temperature and humidity, comparable to the conditions of previous publications.[10,11,15,29,36]

Ultrasonic Echography. At first the longitudinal t_L and transversal t_T sound wave propagation times were determined with an accuracy of ±1 ns by using an echometer (Echometer 1077, Karl Deutsch GmbH & Co. KG) with a piezoelectric transducer (frequency of 8−12 MHz). The longitudinal v_L and transversal v_T sound velocities are calculated using the

https://dx.doi.org/10.1021/acs.jpcc.0c09865
J. Phys. Chem. C 2021, 125, 4183−4195

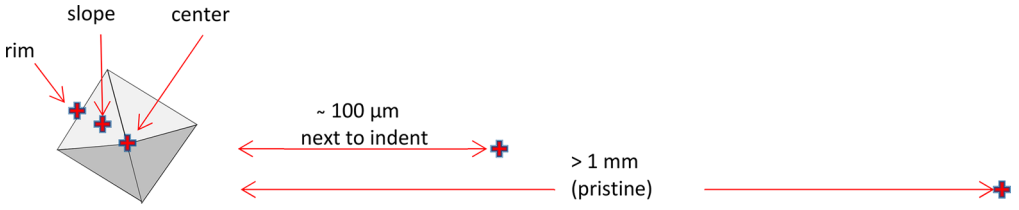

Figure 1. Schematic of the various positions of Raman measurements on indented glass samples. One diagonal of the indent measures ~30 μm (see also Figure 2).

measured specimen thickness d and the time between two consecutive echos:

$$v_L = 2d/t_L$$
$$v_T = 2d/t_T \quad (1)$$

With this information, elastic constants such as the shear modulus G, bulk modulus K, and elastic modulus E as well as the Poisson ratio ν could be calculated by the following equations, which are applicable for isotropic materials (with ρ being the glass density).[37]

$$G = \rho v_T^2 \quad (2)$$

$$K = \rho[v_L^2 - (4/3)v_T^2] \quad (3)$$

$$E = \rho[(3v_L^2 - 4v_T^2)/((v_L/v_T)^2 - 1)] \quad (4)$$

$$\nu = (v_L^2 - 2v_T^2)/2(v_L^2 - v_T^2) \quad (5)$$

Nanoindentation. More information on the mechanical properties was obtained from instrumented indentation testing using a nanoindenter (G200, Agilent Inc.), equipped with a three-sided Berkovich diamond tip operating in the continuous stiffness measurement (CSM) mode. In this setup, the continuously increasing load−displacement signal is superimposed by a small oscillation of the indenter tip (Δh = 2 nm, f = 45 Hz). This setup enables the determination of the depth profiles of hardness H and elastic modulus E by a continuous recording of the indentation depth/displacement into the surface h, the load (on the sample) P, and of the (harmonic) contact stiffness S.[15] On each glass sample, 14 indents of 2 μm depth were generated at a constant strain rate $\dot{\varepsilon}$ of 0.05 s^{-1}. The indents were placed 50 μm apart to avoid the influence of residual stress fields.[38] The resulting load−displacement curves were analyzed using the Oliver-Pharr model.[39] In this method the hardness H is calculated by dividing the load P with the projected contact area of the indenter tip A_C.

$$H = \frac{P}{A_C} \quad (6)$$

The elastic modulus E is derived from the combined elastic response of the tested material and the diamond indenter tip (E_i = 1141 GPa, ν_i = 0.07) by the following formula

$$E = (1 - \nu^2)[(1/E_r) - (1 - \nu_i^2)/E_i] \quad (7)$$

where the reduced elastic modulus E_r is given by the expression

$$E_r = (S/2\beta)(\pi/A_C)^{1/2} \quad (8)$$

where β represents a correction factor[39] that was set to unity for the Berkovich indenter tip used in this study.[15] The contact stiffness of the material S corresponds to the initial slope of the load−displacement curve upon unloading. The contact area A_c was determined prior to the measurements by a calibration of the Berkovich diamond indenter tip on a fused silica reference glass sample. The values for H and E were averaged between the lower 20% (400 nm) and the upper 10% (1800 nm) of each indentation profile/penetration depth profile.

The indentation creep behavior was examined by a nanoindentation strain rate jump test as described by Limbach et al.[15] In this experiment, a three-sided Berkovich diamond tip penetrates the glass surface down to 750 nm with a constant strain rate of 0.05 s^{-1}, until a depth-independent hardness value is achieved. During further penetration the strain rate is alternated every 250 nm from the origin strain rate to the new strain rate and back, and the hardness variation is determined by continuously recording the indentation depth, load, and contact stiffness with the CSM equipment (Δh = 5 nm, f = 45 Hz). Ten tests with strain rates of 0.05, 0.007, and 0.001 s^{-1} were executed on every glass sample, and the corresponding hardness values were averaged over the last 100 nm of each interval. With the assumption of a depth-independent hardness $\left(\frac{\dot{H}}{H} = 0\right)$ the applied strain rate, defined as the loading rate divided by the actual load $\frac{\dot{P}}{P}$, which can then be translated into the indentation strain rate $\dot{\varepsilon}_i$ by[40]

$$\dot{\varepsilon}_i = \frac{\dot{H}}{h} = \frac{1}{2}\left(\frac{\dot{P}}{P} - \frac{\dot{H}}{H}\right) \quad (9)$$

where the parameter $\frac{\dot{H}}{h}$ represents the indentation-rate divided by the actual displacement of the indenter. Subsequently, the logarithm of the hardness $\ln H$ can be plotted against the logarithm of the indentation strain rate $\ln(\dot{\varepsilon}_i)$, and the strain rate sensitivity m can then be derived from the slope of the linear regression curve.[41,42]

$$m = \frac{\partial \ln H}{\partial \ln \dot{\varepsilon}} \quad (10)$$

An increase in the strain rate sensitivity can be treated as the transition from a perfectly rigid plastic material with m = 0 to an ideal Newtonian viscous solid with m = 1.[43,44]

Microindentation. The crack resistance (CR) was approximated by Vickers indentation tests.[2] For this purpose, the glass specimens were indented with stepwise increasing loads, and the number of radial cracks emanating from the corners of the residual imprints were counted. From this, the probability of crack initiation (PCI) was derived as the ratio between the number of corners where a radial crack was formed and the total number of corners on all indents. The PCI was determined for loads between 0.49 and 19.62 N with a microhardness tester (Duramin-1, Struers GmbH). The crack resistance is defined as the load at which an average of two cracks (PCI = 50%) occurred. On every specimen, 25 indents with loading durations of 15 s and dwell times of 10 s were

https://dx.doi.org/10.1021/acs.jpcc.0c09865
J. Phys. Chem. C 2021, 125, 4183−4195

Table 1. Comparison of Physical Properties of ULE, SiO_2, and Duran Glasses[a]

	ULE 7972[b]	ULE	SiO_2	Duran	
ρ (g/cm^3)	2.21	2.21	2.20	2.22	
V_m (cm^3/mol)		27.7	27.31	27.69	
$CTE_{100-300}$ (10^{-6} K^{-1})	0.03[c]		*0.55*[45]	3.3	
shear modulus G (GPa)	29.0	29.2 ± 0.5	29.9 ± 0.5	26.7 ± 0.5	UE
elastic modulus E (GPa)	67.6	68 ± 1.1	70 ± 1.1	64 ± 1.1	UE
bulk modulus K (GPa)	34.1	33.9 ± 0.8	35.4 ± 0.8	35.6 ± 0.8	UE
Poisson ratio υ	0.17	0.165 ± 0.004	0.170 ± 0.004	0.200 ± 0.004	UE
crack resistance (N)		3.72 ± 0.16		4.41	MI
strain rate sensitivity m		0.0104	0.0068	0.0180	NI
hardness H (GPa)		7.66 ± 0.03	9.30 ± 0.12	7.18 ± 0.03	NI

[a]Values in italics are from the literature (as referenced); for mechanical data the experimental set-up is given as *UE:* ultrasonic echography, MI: microindenter; NI: nanoindenter. [b]Data sheet.[32] [c]$CTE_{5-35} = 0 \pm 30 \times 10^{-9}$ K^{-1}.

generated for every load. The cracks were counted directly after unloading and before generating the next indent.

Indentation for the structural studies was conducted in a Vickers geometry using the microhardness tester, providing each specimen with several indents generated with loads of 4.91, 1.96, 0.98, and 0.49 N. A 15 s loading duration and 10 s dwell time was selected, and the indents were placed at least 500 μm apart. Raman measurements were performed the day after indentation as well as weeks later using a different setup, but no significant differences in the spectra was observed for samples measured at different times, when measured at a comparable spot site (see Figure 1).

2.4. Vibrational Spectroscopy. The structural investigations were conducted by Raman spectroscopy and, for pristine glasses, also by reflectance infrared (IR) spectroscopy. Structural changes upon indentation were studied by comparing Raman spectra of pristine glasses with those taken in the indented areas.

Raman. A dispersive confocal micro-Raman spectrometer (inVia Raman Microscope, Renishaw) with the 488 and 514 nm laser excitation lines was used to record the spectrum in the range from 80 to 1600 cm^{-1}. The spectral resolution was 2 cm^{-1}, and the spatial resolution of the micro-Raman was ∼0.5 μm. Some measurements were also conducted with parallel-polarization (HH) or cross-polarization (HV).

Vickers indentation sites with a diameter of up to 30 μm could therefore be probed at different locations of the indent (see also refs 10 and 11 for more details on such Raman studies). All indented samples were measured at four different positions: (a) in the center of the indent, (b) at the slope of the indent, (c) at the rim of the indent, and (d) next to the indent. The positions marked as "next to the indent" were at least 100 μm away from the rim of the indent. To ensure the correctness of these measurements, nonindented reference samples were also analyzed (see Figure 1). Considering that, under the given setup, a 0.5 μm spot on the glass surface of a 30 μm indent diagonal is sampled, the resulting Raman spectrum can be assumed to probe only the modified glass volume and not include much information on any unaffected volume below the indent stress field.

For the Raman spectra of reference materials, we used a WiTec Instrument (Alpha300 confocal Raman spectrometer) with a 50× objective. The resolution was better than 3 cm^{-1}. When the excitation line of 488 nm was used, the power was 20 mW, and integration times varied from 0.5 to 2.5 s, based on 50−200 spectral accumulations.

Reflectance IR Spectroscopy. Pristine glasses were also measured from 30 to 7000 cm^{-1} on a vacuum Fourier transform spectrometer (Vertex 80v, Bruker) in the reflectance mode at nearly normal incidence (11° off-normal). For each sample, measurements were conducted separately in the far- and mid-IR region. The far-IR spectrum is the average of 400 scans, and the mid-IR spectrum is the average of 100 scans, both taken with 2 cm^{-1} resolution. The two spectra were merged to form a continuous reflectance spectrum in the range of 30−7000 cm^{-1} before conversion to absorption coefficient by a Kramers−Kronig transformation.

3. RESULTS AND DISCUSSION

3.1. Mechanical Properties. Selected physical properties of ULE are listed in Table 1. Data for a fully polymerized v-SiO_2, which was studied in parallel to ULE for comparison, and data from ref 10 for the likewise fully polymerized low-alkali borosilicate glass (Duran) are also included in the listing. Measured values for ULE compare well with data from the Corning data sheet.[32]

The measured properties of ULE agree well with the published properties. The density of all three fully polymerized glasses is very close, increasing from 2.20 g/cm^3 in vitreous SiO_2 to 2.21 g/cm^3 in ULE, where heavy titanium replaces every 18th Si-atom, to 2.22 g/cm^3 in Duran, with ∼4 mol % $[BO_4]^-$ and $[AlO_4]^-$ tetrahedra, which are charge-balanced by sodium ions. As the name ULE implies, the coefficient of thermal expansion of ULE is extremely low, an order of magnitude smaller than for silica, for which the CTE is again an order of magnitude less than that of Duran, which is known for its high resistance to thermal shock and is, therefore, used in labware and cooking ware. All three glasses show a high resemblance in their mechanical properties. The shear, elastic, and bulk modulus of SiO_2 is higher, but the values for ULE fall just within the margin of error. The shear and elastic modulus of Duran shows, however, slightly lower values. The Poisson ratio of ULE is slightly lower, though within the error margins of vitreous silica, while Duran shows a slight but significantly higher value. For all three glasses the low Poisson ratio is consistent with their fully polymerized silicate networks, which is related to the anomalous, compaction-driven behavior under indentation.

Photographic images of the crack patterns in ULE glasses after Vicker's indentation are shown in Figure 2. The crack resistance is strictly speaking based on radial cracks, which form upon the indentation of normal glasses such as soda lime silicate glasses, and the given values are therefore only a wide

https://dx.doi.org/10.1021/acs.jpcc.0c09865
J. Phys. Chem. C 2021, 125, 4183−4195

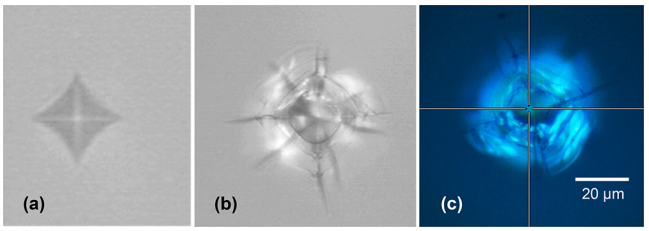

Figure 2. Images using a 40× magnification optical microscope of ULE samples after Vicker's indentation using a load of (a) 491 mN for 10 s and (b) 4.91 N for 30 s. In (c) a similar indent with a load of 4.91 N for a 30 s dwell time is seen under the Raman microscope (50×), where the laser focus appears as a blue spot in the center of the cross-hair. Typical radial-median cracks used for the determination of the CR are visible in (b, c), in addition to cone cracks that are expected for silica.

approximation, and such values are usually not given for silica. The strain rate sensitivity increases and the hardness decreases with decreasing silica content of the three glasses. Both parameters show the most significant changes, though consistent with a highly polymerized glass structure.

3.2. Vibrational Properties of Selected Reference Materials. Before discussing the effect of indentation on the structure of ULE glasses, we need to briefly recap the Raman and IR spectra of pristine vitreous SiO_2 and ULE glass and of reference materials that contain titanium ions in higher than fourfold coordination. A high similarity in the vibrational spectra is expected for both ULE and silica glasses, as tetrahedral titanate units in ULE replace some of the tetrahedral silicate units in the fully polymerized network.[24−26] Figure 3 shows the IR spectra of ULE in comparison with

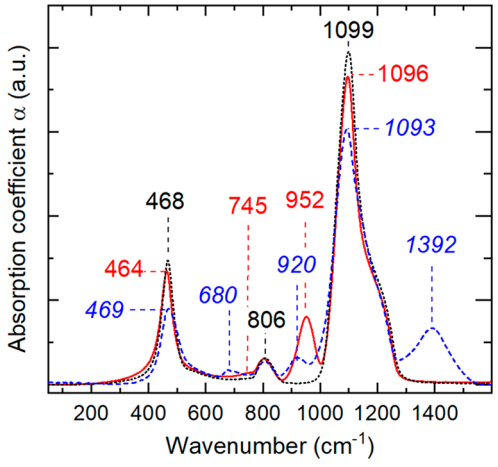

Figure 3. Comparison of infrared absorption spectra of ULE (red, solid line) with vitreous SiO_2 (black, dotted line) and the low-alkali borosilicate glass Duran (blue, broken line). All spectra are normalized to the intensity of the Si−O−Si bending mode at 806 cm^{-1}; stated positions of band maxima for Duran are blue in italics: black for v-SiO_2 and red for ULE.

those of silica and Duran, while Figure 4 depicts the Raman spectra of ULE and other Ti-containing reference materials and Figure 5 compares the Raman spectra of the three fully polymerized glasses ULE, silica, and the Duran-type, low-alkali borosilicate glass before and after indentation. The band assignments for the Raman and IR spectra are based on earlier studies, for example, v-SiO_2[46−51] and ULE.[24] For indentation-

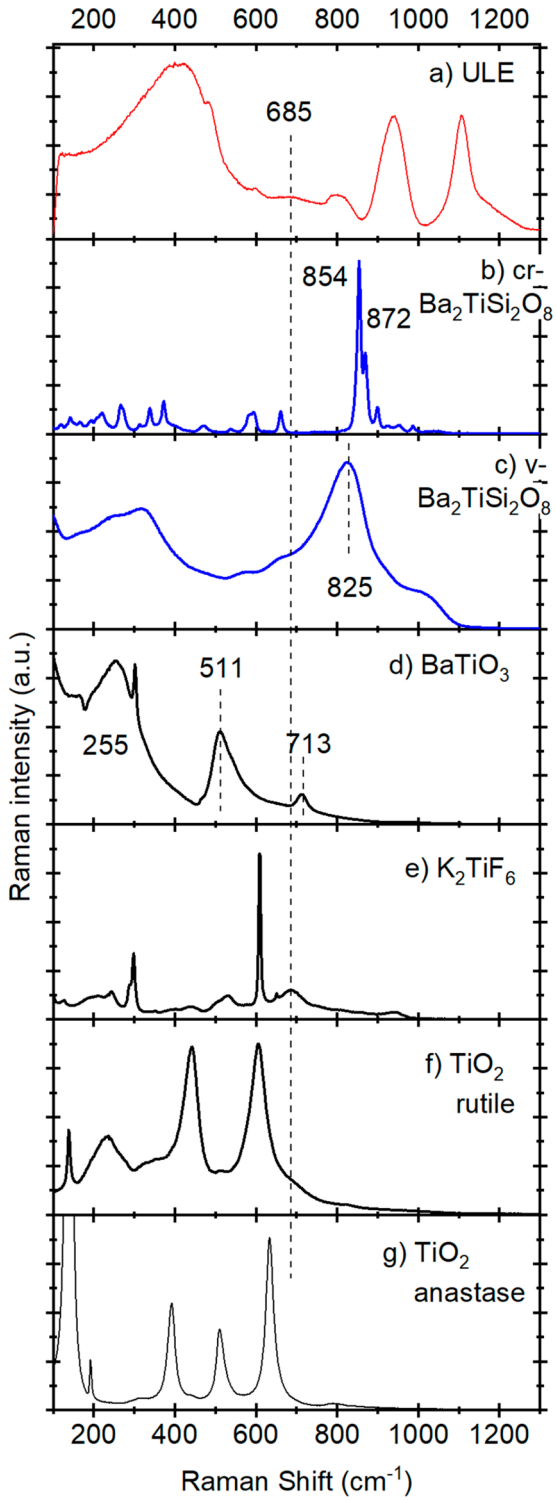

Figure 4. Raman spectra of ULE glass and various titanate reference materials: (a) ULE glass with [4]Ti; (b) devitrified fresnoite $Ba_2TiSi_2O_8$ after heat treatment of the glass sample shown in (c); both contain [5]Ti; (d−g) are samples based on octahedral titanate polyhedra with varying connectivity, [6]Ti. The 488 nm Raman excitation was used; see the text for more details.

induced changes we also refer to our earlier studies on Duran-type borosilicate glasses.[10,11,52,53]

A comparison of Figures 3, 4a, and 5a shows that the effect of small additions of TiO_2 to SiO_2 (only 5.67 mol % in the case of ULE) changes the Raman spectra much more significantly

https://dx.doi.org/10.1021/acs.jpcc.0c09865
J. Phys. Chem. C 2021, 125, 4183−4195

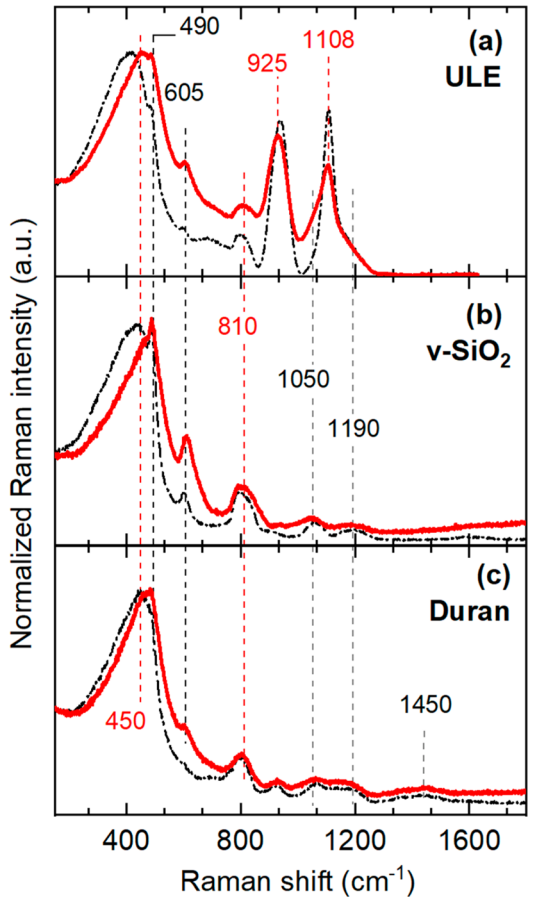

Figure 5. Comparison of Raman spectra before (black broken line) and after indentation probing the center of the indent (red, solid line) of (a) ULE (load: 4.91 N, loading for 30 s), (b) SiO_2, and (c) Duran-type glass (load for both: 4.9 N for 30 s from ref 10). The stated positions of band maxima refer to the spectra after indentation; see Table 2 for pristine samples (the laser excitation wavelength was 488 nm).

than the IR spectra. This can be explained by the higher polarizability of Ti^{4+} (α_{Ti}^{4+} = 0.184 Å^3) compared to Si^{4+} (α_{Si}^{4+} = 0.033 Å^3).[54] These variations in the polarizability translate directly into a higher Raman scattering cross-section for Ti-related bonds. This fact is important to remember, since this means that the Raman spectra emphasize therefore structural variations of the titanate fraction of the glass. IR spectroscopy is not affected by a change in polarizability, as infrared spectroscopy probes a change in the dipole moment (Figure 3).

Figure 3 shows the infrared spectra of the three fully polymerized silica-based glasses. All glasses show as the most dominant feature a band peaking at 1099 cm^{-1} with a shoulder at 1200 cm^{-1}, due to asymmetric stretching vibrations of Si−O−Si bridging bonds in fully polymerized silicate networks. The relative band intensity decreases with decreasing SiO_2 content of the glasses, from v-SiO_2 (100 mol %) to ULE (94 mol %) to Duran (81 mol %). Common to all three glasses are the bending modes of Si−O−Si bridges at 800 cm^{-1} and the network rocking modes peaking at ∼465 cm^{-1}, which are slightly upshifted for the boron-containing glass. ULE and Duran show, as expected, additional features: for ULE, due to titanate, the asymmetric stretching of TiO_4 tetrahedra peaking at 952 cm^{-1},[24] while for Duran the presence of the borate component leads to a feature at 920 cm^{-1} caused by the asymmetric stretching of $[BO_4]^-$ tetrahedra and to the broader band envelope around 1400 cm^{-1} due to an asymmetric stretching of trigonal BO_3 entities.[11,52,53]

The Raman spectra of Figures 4a and 5 show a strong signal, peaking around 400−450 cm^{-1}, due mainly to the symmetric stretching-bending of Si−O−Si bridges in large arrangements including five- to eight-membered silicate ring structures.[51] The band maximum appears at ∼407 cm^{-1} in ULE, 430 cm^{-1} in pure SiO_2, and 450 cm^{-1} in Duran. This band is strongly polarized and disappears in the cross-polarized (HV) spectra.[24] Superimposed on this strong band are weaker sharper peaks at 485 and 600 cm^{-1}, which are assigned to ring-breathing modes of four- and three-membered silicate rings and are known as defect lines D_1 and D_2, respectively.[55] As expected, the symmetric stretching-bending of Si−O−Si bridges and the ring-breathing modes are polarized, and thus their intensity diminishes in the HV spectra.[24] The ring modes are of a significant lower intensity in the ULE compared to pure vitreous SiO_2 glass. When comparing v-SiO_2 with ULE, we note also that the peak frequencies depend on the strength of the involved bonds, which reflects the stiffness of the network. As weaker Ti−O bonds replace stronger Si−O bonds, when a fraction of SiO_2 is substituted by TiO_2, the stretching and bending modes shift to lower frequencies.

In vitreous SiO_2 the next most-intense Raman band corresponds to the bending of Si−O−Si bridges at 800 cm^{-1},[47,48] which is likewise found in ULE and is partially polarized.[24] The asymmetric stretching of Si−O−Si bonds gives a very low intensity in the Raman spectrum of pure SiO_2 at 1060 and 1200 cm^{-1}, which is typical for fully polymerized glasses,[46−48,50] but it gives the strongest feature in the infrared spectrum at 1099 cm^{-1} (Figure 3). A detailed discussion of the TO/LO splitting and slight shifts of the corresponding IR bands and its relation to the Si−O−Si angle in ULE versus SiO_2 can be found in our earlier study.[24]

The most significant change in the Raman spectrum of ULE compared to v-SiO_2 is related to the presence of two high-intensity bands centered at 937 and 1107 cm^{-1}. While the weaker 937 cm^{-1} band is depolarized and, consequently, is also IR active, the 1107 cm^{-1} band is fully polarized and IR-inactive. Another, much weaker, ULE-related Raman band is found at ∼685 cm^{-1}. As discussed earlier,[24] and considering their polarization behavior, we assigned the 937 and 1107 cm^{-1} bands to the asymmetric and symmetric stretching vibrations of TiO_4 tetrahedra, respectively. The weaker Raman band around 685 cm^{-1} might be assigned to a symmetric bending and stretching vibration involving mixed Ti−O−Si bonds. However, bands in this range can also be assigned to a symmetric stretching vibration of TiO_6 octahedral units with Ti−O−Ti bridges.[30,56] Even though earlier XRD studies gave no evidence for the presence of a significant number of directly linked Ti−O−Ti species, a recent diffraction study could not exclude the presence of very small amounts of nontetrahedral species in the ULE.[24]

Figure 4 shows the Raman spectra of a series of reference materials with known titanium coordination and connectivity. As for other MO_x polyhedra, the Ti−O stretching modes of the lower-coordinated species are found at higher frequencies compared to higher-coordinated polyhedra. Thus, the Ti−O stretching modes decrease in frequency in the series of $^{[4]}$Ti > $^{[5]}$Ti > $^{[6]}$Ti [the number in brackets denotes the titanate coordination]. However, the connectivity of the polyhedra also

https://dx.doi.org/10.1021/acs.jpcc.0c09865
J. Phys. Chem. C 2021, 125, 4183−4195

plays an important role, with nonbridging oxygen atoms decreasing the frequency of the corresponding stretching modes, as does a change from corner to edge and to face-sharing oxygen linkages.[57]

Interestingly, in modified silicate-titanate glasses, $^{[6]}$Ti−O−Si bonds might be characterized by high-intensity Raman signals at energies connected with Q^3 stretching modes; by transferring some of the high Ti-related polarizability to the Si−O^- bond, the octahedral Ti^{4+} ion is partially charge balancing. Since the $^{[6]}$Ti−O bond is significantly weaker than the Si−O bond, Raman spectroscopy might show the signal of a depolymerized silicate tetrahedron instead of a Si−O−Ti bridge. As discussed by Su et al.,[56] the high polarizability of titanium ions will be reflected in a high scattering cross-section of the $[O_3Si{-}O]^{\delta-}$—$[TiO_5]^{\delta+}$ linkage. In amorphous and crystalline fresnoite $BaTiSi_2O_8$, a broad band at 825 cm^{-1} or narrower bands at 854 and 873 cm^{-1}, respectively, dominate the spectra.[58,59] This apical short Ti−O bond of the square-planar pyramid of a fivefold coordinated titanium is written as Ti−O* in the literature to distinguish it from the bridging or charge-bearing nonbridging Ti−O bonds, without designating it as a Ti═O double bond. The latter seems to be elusive in solids, where, however, long and short Ti−O bonds have been confirmed.[60] Those titanyl compounds for which a real double bond has been confirmed show a Raman band at 950 cm^{-1} or at higher frequency.[56,60,61] A band at lower frequencies, between 800 and 900 cm^{-1}, is typical for this apical short Ti−O* bond of $^{[5]}$Ti and is also known for silica-free $K_2Ti_2O_5$ crystals, where it peaks at 905 cm^{-1}.[56] In silicate-titanates, this band is overlaid by the activity of silicate tetrahedra with nonbridging oxygen atoms that are charge-balanced by a modifier cation, as the $^{-}[O_3Si{-}O]^{\delta-}$—$[TiO_4]^{\delta+}$ linkage in fresnoite, which from the frequency around 850 cm^{-1} would correspond to Q^2 silicate groups (see Figure 4b,c). Cardinal et al. describe a similar strong Raman signal near 930 cm^{-1}, to signify the presence of the Ti−O* stretch, which was confirmed by extended X-ray absorption fine structure (EXAFS). However, the strong band could also include contributions from a $^{-}[O_3P{-}O]^{\delta-}$—$[TiO_4]^{\delta+}$ linkage for which P−O stretching in broken metaphosphate chains (Q^1_P units) would also appear near a frequency of 930 cm^{-1}.[30] Edge- and face-sharing TiO_6 octahedra are found in rutile and anatase,[62] while $BaTiO_3$ is known to form corner-shared TiO_6 octahedra.[63] The structure of K_2TiF_6 is made of isolated charged TiF_6^{2-} octahedra, which are charge-balanced by K^+ ions in an ionic crystal (Table 2).[64]

3.3. Indentation-Induced Modifications As Probed by Raman Spectroscopy. Indentation was found to induce structural changes in the investigated glasses as has previously been shown for Duran or silica.[10−12,19,22] A comparison of indentation-induced structural changes in the three fully polymerized glasses v-SiO_2, ULE, and Duran is given in Figures 5 and 6, where Raman spectra before and after Vickers indentation are depicted. For all glasses, a shift to higher frequencies is observed for the maximum of the most intense band envelope below 500 cm^{-1}. This is most pronounced in v-SiO_2, where it had been explained by the emergence of a higher number of smaller ring structures upon indentation, compared to a more open structure of larger five- and six-membered rings in the pristine glass.[10,11,51] On the one hand, in the spectrum of Duran, the Si−O−Si stretching-bending mode in the pristine glass has already a narrower form centered at 450 cm^{-1}, and the subsequent upshift after indentation is relatively small, though significant. ULE shows, on the other hand, upon indentation a pronounced upshift of the center of the Si−O−Si stretching-bending modes, though the resulting band envelope is broader and less pointy when compared to that of Duran or v-SiO_2. This finding suggests that the relative population of the smaller four- and three-membered silicate rings is smaller not only in the pristine ULE glass but also in the indented glass, when compared to vitreous SiO_2.

Table 2. Raman Band Assignments for ULE Glass and Various Higher-Coordinated Ti Species

Raman (cm^{-1})	band assignment
ULE	from ref 24
407	symmetric stretching-bending of Si−O−Si bridges in large arrangements such as five- to eight-membered silicate ring structures
484	breathing mode of four-
600	and three-membered silicate rings
685	TiO_6 symmetric stretching
800	Si−O−Si bending
937	TiO_4 asymmetric stretching
1107	TiO_4 symmetric stretching
1060, 1200	Si−O−Si asymmetric stretching
reference materials	
920−960	$^{[6]}$Ti or $^{[5]}$Ti sensibilized Si−O linkages as in a $[O_3Si{-}O]^{\delta-}$—$[TiO_5]^{\delta+}$ type of linkage[56]
829 to 930	Ti═O of $^{[5]}$Ti[30,58,59,65]
740	$^{[6]}$Ti−O−$^{[6]}$Ti chains with Ti−O−Ti linkages[30]
300−600	Bending and stretching modes of edge and face sharing Ti−O−Ti linkages[62]

Structural changes in v-SiO_2 and Duran are mainly limited to the first band envelope, and the only other effect observed upon indentation is an increase in intensity of the ring-breathing mode of three-membered silicate rings at 605 cm^{-1}. While we also observe an increase in the intensity of this D_2-band after an indentation of ULE, this effect is relatively small compared to a broad, relatively unspecific, increase in the Raman activity from ∼650−1000 cm^{-1}. Any increases in the Raman scattering in this range could be related to an increase in the population of higher five- and sixfold coordinated titanium species, which is more compelling when considering a decrease in the intensity of the asymmetric and symmetric TiO_4 stretching modes at 937 and 1107 cm^{-1}, respectively, after indentation (Figure 5a).

Figure 6a shows the structural changes in ULE in more detail, where we compare the Raman spectra of ULE and v-SiO_2 for the same position within the indent after a comparable indentation testing with a load of 4.91 N for 30 s. In Figure 6b, the polarized Raman spectra at four similar locations that are outside the indent, on the rim, slope, and finally in the center of the indent are depicted for ULE (see also the schematic of Figure 1). Figure 6 shows another interesting effect, of the dependence of the intensity of Ti-related bands on the wavelength of the Raman excitation laser line. This resonance Raman enhancement of the titanate compared to the silicate bands is more pronounced when UV laser lines are used for excitation, because they approach the charge-transfer transition of Ti^{4+}-O as discussed in detail in ref 24 for ULE and, earlier, for titanium-silicate zeolites[66] and catalysts.[67,68] The slight difference in the relative band intensities for the spectra of Figure 6a, taken with the 488 nm laser line, compared to the spectra of Figure 5b, which

https://dx.doi.org/10.1021/acs.jpcc.0c09865
J. Phys. Chem. C 2021, 125, 4183−4195

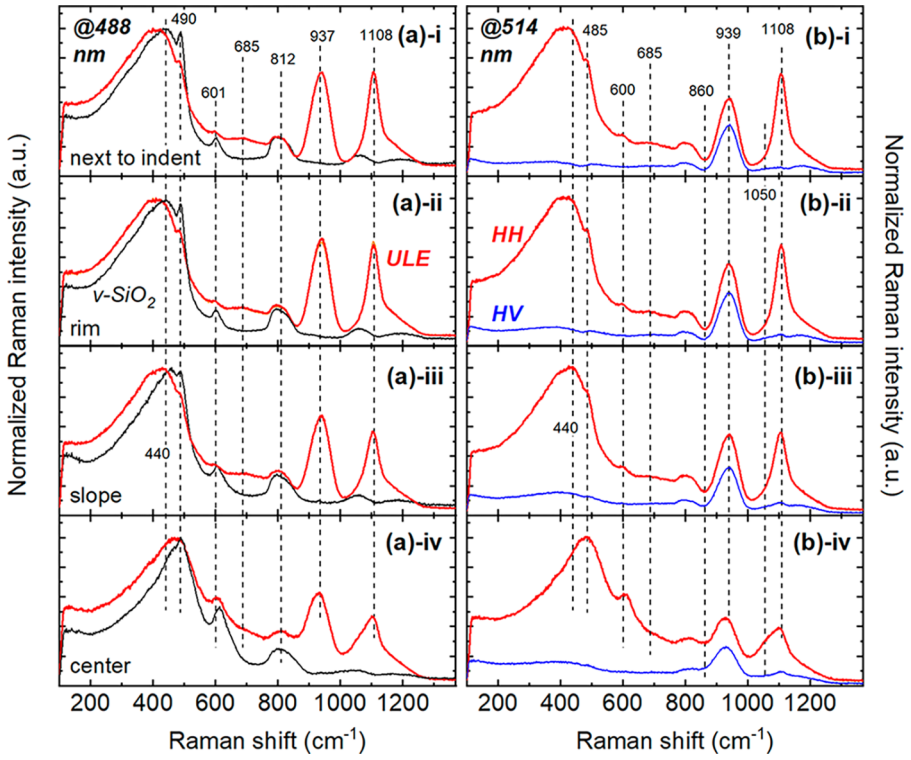

Figure 6. Raman spectra at different positions next to and within the indent; (a) unpolarized Raman spectra of ULE (red, thicker solid lines) in comparison to v-SiO_2 (black, thinner solid lines) and (b) polarized Raman spectra of ULE (red thicker lines: HH, parallel polarization; blue thinner lines: HV, cross-polarization). From top to bottom: (i) pristine or next to indent, (ii) rim, (iii) slope, and (iv) center of indent. Indentation load was 4.91 N for 30 s for both ULE and v-SiO_2. The resonance Raman effect is seen for the unmodified ULE glasses (at the top) as reflected in the different relative intensities of the 937 and 1107 cm^{-1} bands for excitation with the 488 (a) and 514 (b) nm laser lines.

were taken with the 514 nm laser line, is thus explained. The band tail of this charge transfer band is better excited with the shorter wavelengths of the 488 nm laser line than with the slightly longer wavelengths of the 514 nm laser line.

We see a progressive change in the Raman spectra of Figure 6 from the top (i), measured outside the indented area, to the bottom (iv), measured at the center of the indent where the impact of indentation is more pronounced. The observed upshift of the center of gravity of the Si−O−Si stretching-bending band in ULE from ~407 to 470 cm^{-1} (Figure 7) is consistent with earlier findings for the SiO_2 glass,[10,69] and it indicates a decrease in the Si−O−Si bond angle.[51] Also, the indentation of pure silica and the silica-rich titanium silicate causes an increase of the relative intensity of both defect lines D_1 (485 cm^{-1}) and D_2 (600 cm^{-1}) with respect to the activity of the five- to eight-membered rings. Considering the origin of D_1 and D_2, this provides clear evidence that an indentation causes the densification of the silicate network. These structural rearrangements lead altogether to the densification of the silicate (sub)network in the ULE upon indentation.

More complex is the discussion of the observed increase in the Raman activity between 650 and 1000 cm^{-1}, together with the decrease in the band intensity of the TiO_4 stretching modes at 937 and 1107 cm^{-1} (see Figures 4−7). This suggests that, under indentation, titanate tetrahedra are at least distorted, or even transformed into another titanate unit. Interestingly, the decrease in intensity of the asymmetric and symmetric TiO_4 stretching modes does not occur at the same rate; the band at 937 cm^{-1} decreases at a lower rate compared to the 1107 cm^{-1} band.

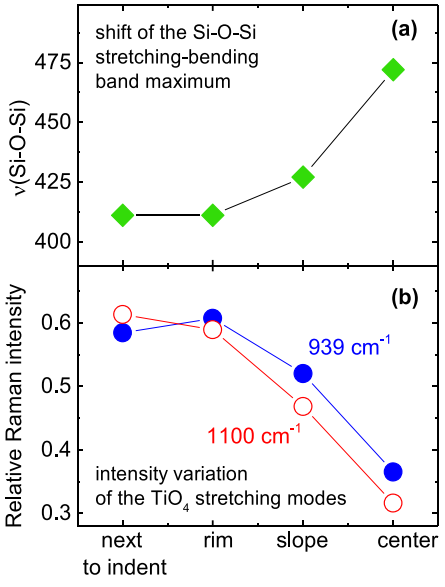

Figure 7. Selected variations in band position and band intensities for different sample positions (see also Figure 1) of ULE after indentation with a load of 4.91 N for 30 s for both (same as Figure 6a): (a) shift of the position of the band maximum of the Si−O−Si stretching-bending band envelope between 400 and 500 cm^{-1}, (b) intensity variation of the symmetric and asymmetric TiO_4 stretching modes (after simple baseline correction to band tails).

https://dx.doi.org/10.1021/acs.jpcc.0c09865
J. Phys. Chem. C 2021, 125, 4183−4195

As seen in Figure 4 and as described in the literature,[30,56] or when considering various published Raman spectra of modified titanate-silicate glasses,[31,70] sixfold coordinated titanate species show bands below 700 cm^{-1}, especially when the materials contain Ti−O−Ti bonds but can reach as high as 950 cm^{-1} when fivefold or octahedral-coordinated titanate polyhedra are bonded to a silicate network. The vibrations of the Ti−O* short apical bond in a fivefold coordinated titanium have been associated with various bands between 800 and 900 cm^{-1}.[30] However, as discussed earlier, it is not clear if this variability of the bond is an actual Ti−O vibration or if it reflects a Si−O bond that has been polarized by linkage to either six- or fivefold coordinated titanium ions, as described by Su et al.[56]

The additional Raman activity arising in the indented ULE (see Figures 4 and 5) cannot be identified as distinct new bands but, rather, as a general increase in the intensity of all features between 650 and 1000 cm^{-1}. In the pristine sample, this activity is much smaller and shows as a distinct feature at ~690 cm^{-1}, which is much weaker than the Raman signatures of TiO_4 tetrahedra at 937 and 1107 cm^{-1}. After indentation, we also see on the lower frequency sides of the symmetric and asymmetric TiO_4 stretching modes the emergence of a Raman shoulder 1050 cm^{-1}, while a broadening and merging of the 812 and 950 cm^{-1} bands leads to an increased Raman activity in the previous minimum at 860 cm^{-1}. These observations are more apparent in the difference spectra shown in Figure 8.

As the intermediate Raman region increases in intensity in the indented ULE glass, the relative band intensities of the stretching modes of TiO_4 tetrahedra at 937 and 1110 cm^{-1} decrease (Figure 7). Also, their peak maxima shift from 937 to ~933 cm^{-1} and from 1110 to ~1105 cm^{-1}. On the basis of the earlier stated Raman assignments, this can be interpreted as a reduced number of TiO_4 tetrahedra after indentation. A similar interpretation was given earlier for a laser modification of ULE glass.[24,28] However, similarities between indented and laser-induced structural changes end here, as the proposed mechanism of laser modification did involve the partial reduction of Ti^{4+} to Ti^{3+} and the oxidation of oxygen ions from the glass network to molecular oxygen aggregated in the laser generated cavities.[24,28] While a change in the titanium ion valence seems dubious upon indentation, a change in coordination is the more likely option.

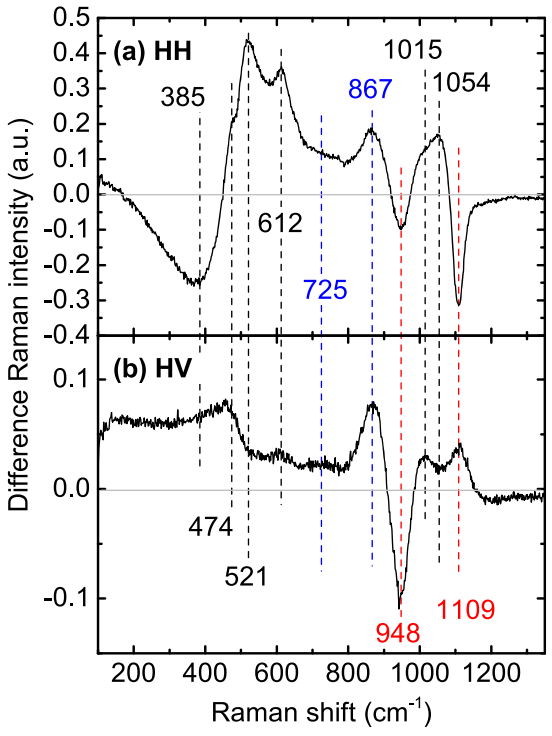

Figure 8. Difference Raman spectra of Figure 6b obtained by subtracting the spectrum next to the indent, Figure 6(b)-i, from the spectrum taken in the center of the indent, Figure 6(b)-iv; (a) parallel polarization and (b) cross-polarization.

Note once again that Raman spectroscopy is less sensitive to changes in the less-polarizable silicate network compared to changes pertaining to the higher-polarizable titanate groups. Thus, we cannot exclude the formation of a small fraction of less-polymerized Q^3 silicate tetrahedra. Large modifications of the silicate network, however, are not apparent, neither in the network deformation nor the bending and stretching modes, while evidence for the presence of higher-coordinated titanate units, TiO_5 and TiO_6 polyhedra, is strong. Unfortunately, infrared spectroscopy lacks the spatial resolution needed for the study of microindentation-induced structural changes. To better understand the changes of the Raman spectra, we plotted in Figure 8 the difference Raman spectra for HH and HV polarizations, obtained after subtracting the corresponding spectrum of the pristine glass (taken next to the indent) from the spectrum at the center of the indent (spectra taken from Figure 6b). As discussed above, we see two distinct minima near 940 and 1110 cm^{-1}, highlighting the decreasing population of TiO_4 tetrahedral units due to indentation. In parallel, a distinct increase in intensity is seen at 867 cm^{-1}, which may indicate the presence of Ti−O* bonds—the shortest apical Ti−O bond in square-pyramidal fivefold-coordinated titanate species. In fresnoite, this band envelope combines the Ti−O* stretch with the symmetric stretching modes of $Si-O^-$ in pyrosilicate dimers.[30,71] A distinct increase is also observed in Figure 8 for the ring-breathing modes of three-membered rings at 612 cm^{-1}. Increases of intensity at 521 and 725 cm^{-1} might be connected to Ti−O−Ti bending and Ti−O stretching modes of corner-sharing octahedra such as are known from $BaTiO_3$.[63] While XRD studies showed no significant number of clustered next-nearest titanate neighbors in pristine ULE, the very weak 685 cm^{-1} had been tentatively assigned to a linked octahedral titanate polyhedral.[24] A significant increase of the titanium coordination, from fourfold to five- and sixfold, would require charge compensation by a formation of titanium clusters or anionic network sites with nonbridging oxygen ions in the silica network, as depicted schematically in Figure 9a,b, respectively. Incidentally, an increase in intensity at 1015 cm^{-1} in the HH polarized spectrum could be indicative of nonbridging oxygen (nbO) formation on silicate Q^2 tetrahedral units, that is, silicate tetrahedra with two nonbridging oxygen atoms with weak linkages to higher-coordinated titanate species (Figure 9b). However, it cannot be excluded that the shoulder at 1015 cm^{-1} in the differential spectra of Figure 6 are merely artifacts from overlapping positive and negative bands.

From all the observed spectral changes of the indent-modified glass structure, we suggest that the dominant process in the deformation behavior of ULE is compaction/densification as observed previously for v-SiO_2. Densification-driven structural rearrangement can result in the formation of

https://dx.doi.org/10.1021/acs.jpcc.0c09865
J. Phys. Chem. C 2021, 125, 4183−4195

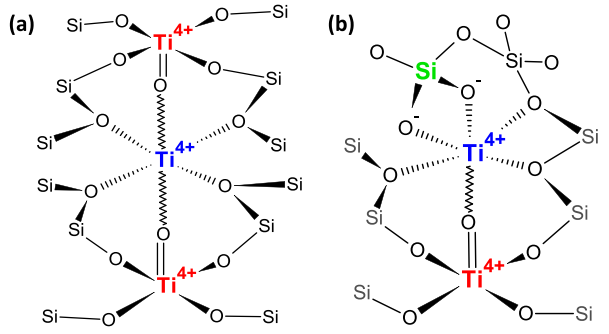

Figure 9. Schematic of a charge-compensated coordination increase of titanium in indented ULE. Solid black bonds (lines or wedge-shaped) are normal single bonds connecting oxygen to silicon, and the difference only indicates the orientation of the connections. Broken, wedge-shaped bonds are ionic in nature, linking oxygen and higher-coordinated titanium ions. The wavelike bond originating from the titanyl ion indicates a dipole bond between the free electron pair of the double-bonded oxygen to the sixfold coordinated Ti^{4+}.

smaller from larger silicate rings. However, contrary to v-SiO_2, a second contribution to the observed densification is due to an increase in the coordination of titanium ions from four- to five- or even sixfold. Since only the TiO_4 tetrahedra are charge-balanced, like SiO_4 tetrahedra with bridging oxygen atoms, we do need to consider proper charge compensation mechanisms to facilitate the formation of higher-coordinated titanium species. The titanyl ion $(O_{4/2}Ti{=}O)^{2-}$ with four bridging and one double-bonded apical oxygen atom, bears formally a doubly negative charge. As depicted in the schematic of Figure 9, an octahedrally coordinated Ti^{4+} ion could contribute—like any other modifier cation—to the charge compensation of the formally negative charges of a titanyl ion.

Statistically, almost 6 of 100 Si^{4+} ions of vitreous silica are replaced by Ti^{4+} ions in ULE. Since titanate and silicate tetrahedra are completely charge-compensated in a fully polymized glass network, the Si and Ti ions would be randomly distributed. However, the stabilization of the proposed titanium species of higher than fourfold coordination (see Figure 9) requires charge compensation by a formation of nonbridging oxygen atoms on the silicate network, some clustering of the few higher coordinated titanate species, or a combination of both processes. A certain rearrangement of bonds is expetected to occur under indentation, as shown by the occurrence of shear bands in glasses,[7] or the breakage of boroxol rings, which has been shown for indented Duran-type glasses.[10] The movement of atoms is required in order to form the indentation crater, and thus, once the high-coordinated titanate species form, they might be permanently stabilized if atomic movement under indentation allows for rearrangement and clustering. This stabilization step is not available for Duran-type glasses, where the tetrahedral borate and threefold coordinated oxygen species are only considered as transient species under high pressures.[10] The more the above-postulated higher-coordinated titanate clusters would of course be facilitated, the more tetrahedrally coordinated titanium ions would already be in close proximity in the pristine glasses. While XRD studies show no evidence for Ti−O−Ti bonds, and considering the presence of one Ti^{4+} for every 18 Si^{4+} in ULE, a random distribution would not favor many Ti−O−Si−O−Ti bonds; it would certainly result in a fraction of Ti−O−Si−O−Si−O−Ti linkages in the pristine glass.

3.4. Structure-Mechanical Property Relation. After having discussed the deformation mechanisms of ULE samples in detail, let us recall the properties listed in Table 1. A ULE usually has properties between those of silica and the low-alkali borosilicate glass of the Duran type. Even though our data were strictly following this trend, experimentally derived values, such as, for example, shear, elastic, and bulk moduli, fall still within the margins of error. As expected, the low Poisson ratio of ULE is consistent with the fully polymerized silicate network and results in a foremost anomalous, compaction-driven behavior under indentation. While the crack resistance is formally lower for ULE compared to Duran, the crack initiation probability curves show that ULE has a much steeper slope for the Weibull distribution of cracks; thus, ULE is resisting cracking to higher loads, where Duran already shows at least one crack. However, once a load is reached where the ULE glass starts to crack, cracks form rapidly near all corners of the Vicker's indent. This behavior is close to that observed for pure silica. Both samples show the formation of cone cracks in addition to small radial cracks, and therefore the conventional method of determining CR might not be fully comparable when applied to fully polymerized anomalous glasses such as SiO_2.

4. CONCLUSIONS

The common structural change observed after indentation in the studied silica-rich glasses SiO_2 and ULE concerns the shift of the main Raman peak around 350−460 cm^{-1} to higher frequencies, which is indicative for a decrease of the Si−O−Si angle. The upshift of this band and the increased intensity of the D_1 and D_2 bands due to four- and three-membered silicate rings, respectively, depend on glass composition and are larger in silica-rich glasses, where densification dominates over a shear-driven deformation. In Duran-type borosilicate glasses, the borate addition offers a pathway of deformation by shear flow via an over coordination of boron and oxygen under the high pressure of the indent. In a ULE, higher-coordinated Ti^{4+} species are not transient but stable even after the high pressure reached during indentation is released. Raman bands connected to fourfold coordinated titanium were found to lose intensity in the indented samples, while the Raman intensity increases in the region of five- and sixfold coordinated titanium species.

Because of charge-balance requirements, the change of titanium from network former as $^{[4]}$Ti to intermediate $^{[5]}$Ti and to network modifier $^{[6]}$Ti triggers the formation of small Ti clusters with up to three Ti atoms with Ti−O−Ti bonding and results in a general increase of Raman scattering below 700 cm^{-1}. Alternatively, modifier-type titanium ions might be charge-balanced by nonbridging oxygen ions on silicate tetrahedra, which, together with the short Ti−O* terminal bond in the TiO_5 square pyramid, would contribute to the Raman signal around 950 cm^{-1}.

AUTHOR INFORMATION

Corresponding Author

Doris Möncke − *Inamori School of Engineering at the New York State College of Ceramics, Alfred University, 14802 Alfred, New York, United States;* orcid.org/0000-0002-4197-5520; Phone: +1 (607) 871-2498; Email: moncke@aldfred.edu

https://dx.doi.org/10.1021/acs.jpcc.0c09865
J. Phys. Chem. C 2021, 125, 4183−4195

Authors

Felix Lind − *Otto-Schott-Institute of Materials Research, Friedrich-Schiller-University Jena, 07743 Jena, Germany*

Brian Topper − *Inamori School of Engineering at the New York State College of Ceramics, Alfred University, 14802 Alfred, New York, United States*

Efstratios I. Kamitsos − *Theoretical and Physical Chemistry Institute, National Hellenic Research Foundation, 11635 Athens, Greece;* orcid.org/0000-0003-4667-2374

Complete contact information is available at: https://pubs.acs.org/10.1021/acs.jpcc.0c09865

Notes

The authors declare no competing financial interest.

■ ACKNOWLEDGMENTS

We gratefully acknowledge financial support through the Priority Program 1594 of the German Science Foundation under Grant No. MO1375/3-1 and through the joint DAAD-IKYDA 2015 program for fostering exchange between German and Greek universities (Grant No. 57161434). E.I.K. also acknowledges support by the project "National Infrastructure in Nanotechnology, Advanced Materials and Micro-/Nano-electronics" (MIS 5002772), funded by the Operational Program "Competitiveness, Entrepreneurship and Innovation" (NSRF 2014-2020) and cofinanced by Greece and the European Union (European Regional Development Fund). Most of the experiments on ULE have been conducted at the NHRF in Athens, Greece and, for reference materials, at Alfred University. Part of this material (Raman data) is based upon work supported by the National Science Foundation under Grant No. DMR-1626164. Indentation and mechanical testing was conducted at the Otto-Schott-Institute of Materials Research at the Friedrich-Schiller University in Jena, Germany, when F.L. and D.M. were members of the glass group of L. Wondraczek. For helpful discussions and/or experimental help, we thank I. Efthimiopoulos, D. Ehrt, J. Hunt, D. Palles, R. Limbach, and F. Zimmermann.

■ REFERENCES

(1) Wada, M.; Furukawa, H.; Fujita, K. Crack resistance of glass on Vickers indentation. *Proc. Int. Congr. Glass* **1974**, 39−46.

(2) Kato, Y.; Yamazaki, H.; Yoshida, S.; Matsuoka, J. Effect of densification on crack initiation under Vickers indentation test. *J. Non-Cryst. Solids* **2010**, *356* (35−36), 1768−1773.

(3) Yoshida, S. Indentation deformation and cracking in oxide glass − toward understanding of crack nucleation. *J. Non-Cryst. Solids: X* **2019**, *1*, 100009.

(4) Rouxel, T.; Yoshida, S. The fracture toughness of inorganic glasses. *J. Am. Ceram. Soc.* **2017**, *100* (10), 4374−4396.

(5) Yoshida, S.; Wada, K.; Fujimura, T.; Yamada, A.; Kato, M.; Matsuoka, J.; Soga, N., Evaluation of sinking-in and cracking behavior of soda-lime glass under varying angle of trigonal pyramid indenter. *Front. Mater.* **2016**, *3* (54). DOI: 10.3389/fmats.2016.00054

(6) Rouxel, T. Driving force for indentation cracking in glass: composition, pressure and temperature dependence. *Philos. Trans. R. Soc., A* **2015**, *373* (2038), 20140140.

(7) Januchta, K.; Smedskjaer, M. M. Indentation deformation in oxide glasses: Quantification, structural changes, and relation to cracking. *J. Non-Cryst. Solids: X* **2019**, *1*, 100007.

(8) Rouxel, T. Elastic properties and short-to medium-range order in glasses. *J. Am. Ceram. Soc.* **2007**, *90* (10), 3019−3039.

(9) Kurkjian, C. R.; Gupta, P. K.; Brow, R. K. The strength of silicate glasses: What do we know, what do we need to know? *Int. J. Appl. Glass Sci.* **2010**, *1* (1), 27−37.

(10) Winterstein-Beckmann, A.; Möncke, D.; Palles, D.; Kamitsos, E. I.; Wondraczek, L. Raman spectroscopic study of structural changes induced by micro-indentation in low alkali borosilicate glasses. *J. Non-Cryst. Solids* **2014**, *401* (0), 110−114.

(11) Winterstein-Beckmann, A.; Möncke, D.; Palles, D.; Kamitsos, E. I.; Wondraczek, L. A Raman-spectroscopic study of indentation-induced structural changes in technical alkali-borosilicate glasses with varying silicate network connectivity. *J. Non-Cryst. Solids* **2014**, *405* (0), 196−206.

(12) Arora, A.; Marshall, D. B.; Lawn, B. R.; Swain, M. V. Indentation deformation/fracture of normal and anomalous glasses. *J. Non-Cryst. Solids* **1979**, *31* (3), 415−428.

(13) Januchta, K.; Youngman, R. E.; Goel, A.; Bauchy, M.; Rzoska, S. J.; Bockowski, M.; Smedskjaer, M. M. Structural origin of high crack resistance in sodium aluminoborate glasses. *J. Non-Cryst. Solids* **2017**, *460*, 54−65.

(14) Bruns, S.; Uesbeck, T.; Weil, D.; Möncke, D.; van Wüllen, L.; Durst, K.; de Ligny, D., Influence of Al_2O_3 addition on structure and mechanical properties of borosilicate glassesInfluence of Al_2O_3 addition on structure and mechanical properties of borosilicate glasses. *Front. Mater.* **2020**. DOI: 10.3389/fmats.2020.00189

(15) Limbach, R.; Rodrigues, B. P.; Wondraczek, L. Strain-rate sensitivity of glasses. *J. Non-Cryst. Solids* **2014**, *404*, 124−134.

(16) Kermouche, G.; Barthel, E.; Vandembroucq, D.; Dubujet, P. Mechanical modelling of indentation-induced densification in amorphous silica. *Acta Mater.* **2008**, *56* (13), 3222−3228.

(17) Perriot, A.; Vandembroucq, D.; Barthel, E.; Martinez, V.; Grosvalet, L.; Martinet, C.; Champagnon, B. Raman microspectroscopic characterization of amorphous silica plastic behavior. *J. Am. Ceram. Soc.* **2006**, *89* (2), 596−601.

(18) Kassir-Bodon, A.; Deschamps, T.; Martinet, C.; Champagnon, B.; Teisseire, J.; Kermouche, G. Raman mapping of the indentation-induced densification of a soda-lime-silicate glass. *Int. J. Appl. Glass Sci.* **2012**, *3* (1), 29−35.

(19) Yoshida, S.; Nishikubo, Y.; Konno, A.; Sugawara, T.; Miura, Y.; Matsuoka, J. Fracture- and indentation-induced structural changes of sodium borosilicate glasses. *Int. J. Appl. Glass Sci.* **2012**, *3* (1), 3−13.

(20) Malchow, P.; Johanns, K. E.; Möncke, D.; Korte-Kerzel, S.; Wondraczek, L.; Durst, K. Composition and cooling-rate dependence of plastic deformation, densification, and cracking in sodium borosilicate glasses during pyramidal indentation. *J. Non-Cryst. Solids* **2015**, *419* (0), 97−109.

(21) Zehnder, C.; Bruns, S.; Peltzer, J.-N.; Durst, K.; Korte-Kerzel, S.; Möncke, D., Influence of cooling rate on cracking and plastic deformation during impact and indentation of borosilicate glasses. *Front. Mater.* **2017**, *4* (5). DOI: 10.3389/fmats.2017.00005

(22) Zehnder, C.; Peltzer, J.-N.; Gibson, J. S. K. L.; Möncke, D.; Korte-Kerzel, S. Non-Newtonian flow to the theoretical strength of glasses via impact nanoindentation at room temperature. *Sci. Rep.* **2017**, *7* (1), 17618.

(23) Gerlich, D.; Wolf, M.; Yaacov, I.; Nissenson, B. Thermoelastic properties of ULE® titanium silicate glass. *J. Non-Cryst. Solids* **1976**, *21* (2), 243−249.

(24) Efthimiopoulos, I.; Palles, D.; Richter, B.; Hoppe, U.; Möncke, D.; Wondraczek, L.; Nolte, S.; Kamitsos, E. I. Femtosecond laser-induced transformations in ultra-low expansion glass: Microstructure and local density variations by vibrational spectroscopy. *J. Appl. Phys.* **2018**, *123* (23), 233105.

(25) Sandstrom, D. R.; Lytle, F. W.; Wei, P. S. P.; Greegor, R. B.; Wong, J.; Schultz, P. Coordination of Ti in TiO_2-SiO_2 glass by X-ray absorption spectroscopy. *J. Non-Cryst. Solids* **1980**, *41* (2), 201−207.

(26) Greegor, R. B.; Lytle, F. W.; Sandstrom, D. R.; Wong, J.; Schultz, P. Investigation of TiO_2-SiO_2 glasses by X-ray absorption spectroscopy. *J. Non-Cryst. Solids* **1983**, *55* (1), 27−43.

(27) Richter, S.; Miese, C.; Döring, S.; Zimmermann, F.; Withford, M. J.; Tünnermann, A.; Nolte, S. Laser induced nanogratings beyond fused silica - periodic nanostructures in borosilicate glasses and ULE. *Opt. Mater. Express* **2013**, *3* (8), 1161−1166.

(28) Richter, S.; Möncke, D.; Zimmermann, F.; Kamitsos, E. I.; Wondraczek, L.; Tünnermann, A.; Nolte, S. Ultrashort pulse induced modifications in ULE - from nanograting formation to laser darkening. *Opt. Mater. Express* **2015**, *5* (8), 1834−1850.
(29) Grammes, T.; Limbach, R.; Bruns, S.; van Wüllen, L.; de Ligny, D.; Kamitsos, E. I.; Durst, K.; Wondraczek, L.; Brauer, D. S., Tailoring the mechanical properties of metaluminous aluminosilicate glasses by phosphate incorporation. *Front. Mater.* **2020**, *7* (115). DOI: 10.3389/fmats.2020.00115
(30) Cardinal, T.; Fargin, E.; Le Flem, G.; Couzi, M. Raman scattering and XAFS study of optically nonlinear glasses of the TiO_2-$NaPO_3$-$Na_2B_4O_7$ system. *J. Solid State Chem.* **1995**, *120* (1), 151−156.
(31) Nienhuis, E. T.; Marcial, J.; Robine, T.; Le Losq, C.; Neuville, D. R.; Stennett, M. C.; Hyatt, N. C.; McCloy, J. S. Effect of Ti^{4+} on the structure of nepheline ($NaAlSiO_4$) glass. *Geochim. Cosmochim. Acta* **2020**, *290*, 333−351.
(32) Corning. Ultra Low Expansion Glass, Advanced Optics and Materials. In *ULE® Corning Code 7972;* Corning Inc., 2016.
(33) Heraeus. *Quartz glass for optics data and properties;* Heraeus Quarzglas GmbH & Co. KG, 2016.
(34) Januchta, K.; Stepniewska, M.; Jensen, L. R.; Zhang, Y.; Somers, M. A. J.; Bauchy, M.; Yue, Y.; Smedskjaer, M. M. Breaking the limit of micro-ductility in oxide glasses. *Advanced Science* **2019**, *6* (18), 1901281.
(35) Pönitzsch, A.; Nofz, M.; Wondraczek, L.; Deubener, J. Bulk elastic properties, hardness and fatigue of calcium aluminosilicate glasses in the intermediate-silica range. *J. Non-Cryst. Solids* **2016**, *434*, 1−12.
(36) Bechgaard, T. K.; Mauro, J. C.; Smedskjaer, M. M. Time and humidity dependence of indentation cracking in aluminosilicate glasses. *J. Non-Cryst. Solids* **2018**, *491*, 64−70.
(37) Sellappan, P.; Rouxel, T.; Celarie, F.; Becker, E.; Houizot, P.; Conradt, R. Composition dependence of indentation deformation and indentation cracking in glass. *Acta Mater.* **2013**, *61* (16), 5949−5965.
(38) Hay, J. Introduction to instrumented indentation testing. *Exp. Techniques* **2009**, *33* (6), 66−72.
(39) Oliver, W. C.; Pharr, G. M. An improved technique for determining hardness and elastic modulus using load and displacement sensing indentation experiments. *J. Mater. Res.* **1992**, *7* (06), 1564−1583.
(40) Lucas, B. N.; Oliver, W. C. Indentation power-law creep of high-purity indium. *Metall. Mater. Trans. A* **1999**, *30* (3), 601−610.
(41) Shen, L.; Cheong, W. C. D.; Foo, Y. L.; Chen, Z. Nanoindentation creep of tin and aluminium: A comparative study between constant load and constant strain rate methods. *Mater. Sci. Eng., A* **2012**, *532*, 505−510.
(42) Maier, V.; Merle, B.; Göken, M.; Durst, K. An improved long-term nanoindentation creep testing approach for studying the local deformation processes in nanocrystalline metals at room and elevated temperatures. *J. Mater. Res.* **2013**, *28* (9), 1177−1188.
(43) Bower, A. F.; Fleck, N. A.; Needleman, A.; Ogbonna, N. Indentation of a power law creeping solid. *Proc. R. Soc. London, Ser. A: Mathematical Physical and Engineering Sciences* **1993**, *441* (1911), 97−124.
(44) Goodall, R.; Clyne, T. W. A critical appraisal of the extraction of creep parameters from nanoindentation data obtained at room temperature. *Acta Mater.* **2006**, *54* (20), 5489−5499.
(45) Weber, M. J. Optical Properties of Glasses. In *Materials Science and Technology;* Wiley-VCH Verlag GmbH & Co. KGaA, 2006. DOI: 10.1002/9783527603978.mst0101
(46) Galeener, F. L. Band limits and the vibrational spectra of tetrahedral glasses. *Phys. Rev. B: Condens. Matter Mater. Phys.* **1979**, *19* (8), 4292−4297.
(47) Galeener, F. L.; Leadbetter, A. J.; Stringfellow, M. W. Comparison of the neutron, Raman, and infrared vibrational-spectra of vitreous SiO_2, GeO_2, and BeF_2. *Phys. Rev. B: Condens. Matter Mater. Phys.* **1983**, *27* (2), 1052−1078.
(48) Kamitsos, E. I.; Patsis, A. P.; Kordas, G. Infrared-reflectance spectra of heat-treated sol-gel-derived silica. *Phys. Rev. B: Condens. Matter Mater. Phys.* **1993**, *48* (17), 12499−12505.
(49) Kamitsos, E. I. Infrared-reflectance spectra of heat-treated, sol-gel-derived silica - Reply. *Phys. Rev. B: Condens. Matter Mater. Phys.* **1996**, *53* (21), 14659−14662.
(50) Pasquarello, A.; Car, R. Identification of Raman defect lines as signatures of ring structures in vitreous silica. *Phys. Rev. Lett.* **1998**, *80* (23), 5145−5147.
(51) Furukawa, T.; Fox, K. E.; White, W. B. Raman spectroscopic investigation of the structure of silicate glasses. III. Raman intensities and structural units in sodium silicate glasses. *J. Chem. Phys.* **1981**, *75* (7), 3226−3237.
(52) Möncke, D.; Ehrt, D.; Varsamis, C.-P. E.; Kamitsos, E. I.; Kalampounias, A. G. Thermal history of a low alkali borosilicate glass probed by infrared and Raman spectroscopy. *Glass Technol. - Eur. J. Glass Sci. Technol. Part A* **2006**, *47* (5), 133−137.
(53) Möncke, D.; Ehrt, D.; Kamitsos, E. I. Spectroscopic study of manganese-containing borate and borosilicate glasses: cluster formation and phase separation. *Phys. Chem. Glasses - Eur. J. Glass Sci. Technol. B* **2013**, *54* (1), 42−51.
(54) Dimitrov, V.; Sakka, S. Electronic oxide polarizability and optical basicity of simple oxides. I. *J. Appl. Phys.* **1996**, *79* (3), 1736−1740.
(55) Barrio, R. A.; Galeener, F. L.; Martinez, E.; Elliott, R. J. Regular ring dynamics in AX_2 tetrahedral glasses. *Phys. Rev. B: Condens. Matter Mater. Phys.* **1993**, *48* (21), 15672−15689.
(56) Su, Y.; Balmer, M. L.; Bunker, B. C. Raman spectroscopic studies of silicotitanates. *J. Phys. Chem. B* **2000**, *104* (34), 8160−8169.
(57) Tarte, P.; Rulmont, A.; Liégeois-Duyckaerts, M.; Cahay, R.; Winand, J. M. Vibrational spectroscopy and solid state chemistry. *Solid State Ionics* **1990**, *42* (3), 177−196.
(58) Markgraf, S. A.; Sharma, S. K.; Bhalla, A. S. Raman study of fresnoite-type materials: Polarized single crystal, crystalline powders, and glasses. *J. Mater. Res.* **1993**, *8* (3), 635−648.
(59) Gabelica-Robert, M.; Tarte, P. Vibrational spectrum of fresnoite ($Ba_2TiOSi_2O_7$) and isostructural compounds. *Phys. Chem. Miner.* **1981**, *7* (1), 26−30.
(60) Noda, L. K.; Sensato, F. R.; Gonçalves, N. S. Titanyl sulphate, an inorganic polymer: Structural studies and vibrational assignment. *Quim. Nova* **2019**, *42*, 1112−1115.
(61) Bamberger, C. E.; Begun, G. M.; MacDougall, C. S. Raman spectroscopy of potassium titanates: Their synthesis, hydrolytic reactions, and thermal stability. *Appl. Spectrosc.* **1990**, *44* (1), 30−37.
(62) Zhang, J.; Li, M.; Feng, Z.; Chen, J.; Li, C. UV Raman spectroscopic study on TiO_2. I. Phase transformation at the surface and in the bulk. *J. Phys. Chem. B* **2006**, *110* (2), 927−935.
(63) Lazarević, Z. Ž.; Vijatović, M. M.; Stojanović, B. D.; Romčević, M. J.; Romčević, N. Ž. Structure study of nanosized La- and Sb-doped $BaTiO_3$. *J. Alloys Compd.* **2010**, *494* (1), 472−475.
(64) Lv, L.; Chen, Z.; Liu, G.; Huang, S.; Pan, Y. Optimized photoluminescence of red phosphor K_2TiF_6:Mn^{4+} synthesized at room temperature and its formation mechanism. *J. Mater. Chem. C* **2015**, *3* (9), 1935−1941.
(65) Markgraf, S. A.; Sharma, S. K.; Bhalla, A. S. Raman Study of Glasses of $Ba_2TiSi_2O_8$ and $Ba_2TiGe_2O_8$. *J. Am. Ceram. Soc.* **1992**, *75* (9), 2630−2632.
(66) Su, J.; Xiong, G.; Zhou, J.; Liu, W.; Zhou, D.; Wang, G.; Wang, X.; Guo, H. Amorphous Ti species in titanium silicalite-1: Structural features, chemical properties, and inactivation with sulfosalt. *J. Catal.* **2012**, *288*, 1−7.
(67) Ricchiardi, G.; Damin, A.; Bordiga, S.; Lamberti, C.; Spanò, G.; Rivetti, F.; Zecchina, A. Vibrational structure of titanium silicate catalysts. A spectroscopic and theoretical study. *J. Am. Chem. Soc.* **2001**, *123* (46), 11409−11419.
(68) Bordiga, S.; Damin, A.; Bonino, F.; Ricchiardi, G.; Zecchina, A.; Tagliapietra, R.; Lamberti, C. Resonance Raman effects in TS-1: the structure of Ti(iv) species and reactivity towards H_2O, NH_3 and

H_2O_2: an in situ study. *Phys. Chem. Chem. Phys.* **2003**, *5* (20), 4390−4393.
(69) Deschamps, T.; Kassir-Bodon, A.; Sonneville, C.; Margueritat, J.; Martinet, C.; de Ligny, D.; Mermet, A.; Champagnon, B. Permanent densification of compressed silica glass: a Raman-density calibration curve. *J. Phys.: Condens. Matter* **2013**, *25* (2), 025402.
(70) Scannell, G.; Barra, S.; Huang, L. Structure and properties of Na_2O-TiO_2-SiO_2 glasses: Role of Na and Ti on modifying the silica network. *J. Non-Cryst. Solids* **2016**, *448*, 52−61.
(71) Varshal, B. G.; Denisov, V. N.; Mavrin, B. N.; Podobedov, V. B.; Sterin, K. E. Hyper-Raman scattering spectra of the glass systems TiO_2-SiO_2, Na_2O-SiO_2, and Na_2O-TiO_2-SiO_2. *J. Appl. Spectrosc.* **1980**, *32* (3), 270−273.

NOTE ADDED AFTER ASAP PUBLICATION

This paper was published ASAP on February 10, 2021, with errors in the Abstract and Figure 4 caption. The corrected version was reposted on February 15, 2021.

https://dx.doi.org/10.1021/acs.jpcc.0c09865
J. Phys. Chem. C 2021, 125, 4183−4195